False-Color Display of Special Sensor Microwave/Imager (SSM/I) Data

Andrew J. Negri,*
Robert F. Adler,*
and Christian D. Kummerow*†

Abstract

Displays of multi-frequency passive microwave data from the Special Sensor Microwave/Imager (SSM/I) flying on the Defense Meteorological Satellite Program (DMSP) spacecraft are presented. Observed brightness temperatures at 85.5 GHz (vertical and horizontal polarizations) and 37 GHz (vertical polarization) are respectively used to "drive" the red, green, and blue "guns" of a color monitor. The resultant false-color images can be used to distinguish land from water, highlight precipitation processes and structure over both land and water, and detail variations in other surfaces such as deserts, snow cover, and sea ice. The observations at 85.5 Ghz also add a previously unavailable frequency to the problem of rainfall estimation from space. Examples of mesoscale squall lines, tropical and extra-tropical storms, and larger-scale land and atmospheric features as "viewed" by the SSM/I are shown.

1. Introduction

Data from the Special Sensor Microwave/Imager (SSM/I) on board the recently launched Defense Meteorological Satellite Program (DMSP) satellite[1] are proving to be a rich source of information in both operations and research. The Department of Defense (DOD) and the National Oceanographic and Atmospheric Administration (NOAA) are, for example, utilizing the data to calculate cloud-water content, precipitation rates, and sea-ice concentration. Researchers are also examining the data to better understand a wide spectrum of atmospheric, oceanographic, and land-surface phenomena, such as vegetation cover, soil moisture, and surface temperature. The continuous operation and wider swath of the SSM/I, compared to the now defunct NIMBUS-7 Scanning Multi-frequency Microwave Radiometer (SSMR)[2] will allow for greater continuity in observations of the earth made in the microwave portion of the spectrum and will be especially beneficial in studies of precipitation, storms, and other highly variable phenomena. The SSM/I "views" the earth's surface over a 1400-km wide swath, and measures polarized microwave emissions at 19.35, 22.24, 37.0, and 85.5 GHz. Particularly important are the 85.5 GHz channels, which expand the range of microwave frequencies observed from space. The current SSM/I is the first in a series of identical instruments to be flown on the DMSP satellites, and so there is a potential for a long record of observation for climate studies. Table 1 shows the seven SSM/I channels, their resolution, and their spatial sampling. A detailed description of the SSM/I may be found in Hollinger et al. (1987).

A method for displaying microwave data from the SSM/I as false-color images[3] is presented here. Brightness temperatures (T_B) observed at 85.5 GHz (vertical and horizontal polarizations) and at 37 GHz (vertical polarization) are displayed simultaneously on a color monitor through the red, green, and blue (RGB) guns. The images highlight qualitatively geophysical parameters important in a wide range of disciplines. In the following sections a brief description of the characteristics of microwave radiation, a description of the false-color technique, and examples of the imagery generated from the SSM/I are given.

2. Some basics of microwave radiation

At microwave frequencies, the power emitted by a body in radiative equilibrium is almost directly proportional to its blackbody temperature (T_{BB}). The actual power emitted is that of a blackbody multiplied by its emissivity (ε), or, using T_{BB} instead of power, εT_{BB}. This power may be expressed in terms of a brightness temperature (T_B), which is proportional to the actual power emitted ($T_B = \varepsilon T_{BB}$).

* Laboratory for Atmospheres, NASA/Goddard Space Flight Center, Greenbelt, MD 20771
† Universities Space Research Association

[1] The DMSP satellite is in a sun-synchronous orbit at a height of 833 km that is inclined 98.8° to the equatorial plane. Its orbital period is 102 min, or 14.1 orbits/day. Local equator-crossing times are 0612 and 1812.

[2] See Prabhakara et al. (1986) or Spencer et al. (1983).

[3] Petersen et al. (1984) delineated regions of convective instability though innovative use of false-color geosynchronous satellite imagery. Earth resources applications of the technique may be found in Short et al. (1976) or in Colwell (1983). D'Entremont and Thomason (1987) used false-color displays of multispectral infrared imagery from the NOAA-7 AVHRR to improve automated cloud analysis.

TABLE 1. Spatial resolution of SSM/I channels. Adapted from Hollinger et al. (1987).

Frequency (GHz)	Polarization	Resolution Along-track (km)	Resolution Cross-track (km)	Spatial sampling (km)
19.35	vertical	69	43	25
19.35	horizontal	69	43	25
22.235	vertical	50	40	25
37.0	vertical	37	28	25
37.0	horizontal	37	29	25
85.5	vertical	15	13	12.5
85.5	horizontal	15	13	12.5

a. Water surfaces

The ocean has a low emissivity (of the order 0.5) that does not vary markedly. The T_B observed over cloud-free warm oceans is therefore ~150 K, rather than say 300 K. The energy emitted from a water surface is polarized. For a viewing angle of 50°, 0.4 and 0.6 are typical values for the horizontal and vertical emissivity.

b. Land surfaces

Land surfaces tend to have high emissivities (near 1.0). On the length scale of the microwave radiation (~1 cm), the land is very rough; thus surface polarization effects are small.[4] On land the emissivity also depends on the vegetative cover, soil type, and soil moisture.

c. Snow cover

Emission from snow-covered ground, though unpolarized, is strongly affected by the moisture content of the snow. Dry snow has a low emissivity (~0.6) at 37 GHz, resulting in low T_B. Wet snow may have emissivities in the range 0.8–0.95.

d. Sea ice[5]

Emission from first-year ice (a homogeneous surface) is similar to that from land or wet snow: characterized by high emissivity, but different in regard to its polarization. Observations in the SSM/I 85.5 GHz channels indicate polarization differences of some 14 K off the coast of Labrador (see cover figure). As ice ages, inhomogeneities increase, decreasing both the emissivity and the polarization difference.

e. Atmospheric effects

Atmospheric constituents such as water vapor, cloud water, and rain radiate power at their equilibrium temperature. The difference between a "cold" ocean background (150 K) and the relatively "warm" emission from these constituents is ideal for their detection and quantification. Over the usually warm land background, the thermal-emission characteristics of atmospheric constituents are difficult to detect.

Large raindrops and ice particles, such as graupel or hail, scatter microwave radiation, effectively lowering the background brightness temperature by scattering emitted radiation away from the satellite. This effect is most pronounced at high frequencies at which the particle size becomes comparable to the wavelength. This lowering of the T_B due to scattering by precipitation-sized hydrometeors is equally effective over water and land. The relationship, though indirect, between this scattering process and surface rain-rate, enables the 85.5 GHz observations to play a key role in identifying precipitation. This capability has already been shown using aircraft microwave data at 92 GHz (Wilheit et al. 1982, Hakkarinen and Adler 1988, Heymsfield and Fulton 1988), by analysis of coupled radiative transfer/numerical cloud models (Adler et al. 1988), and by preliminary analysis of SSM/I data (Spencer et al. 1988). These relationships can also be seen in the calculations of Wu and Weinman (1984).

3. False-color image displays

Brightness temperatures in the SSM/I wavelengths (19–86 GHz) have been observed to be between 80 K and 320 K. To drive each "gun" on the National Aeronautics and Space Administration's (NASA's) Atmospheric and Oceanographic Information Processing System (AOIPS), the input data must be an integer between 0 and 255. For the SSM/I data this is accomplished by choosing $C = 305 - T_B$ where C is the integer to be input to an AOIPS gun and T_B is the observed brightness temperature at a particular SSM/I wavelength. T_B less than 50 K (not yet observed) would be set to a count of 255, while T_B greater than 305 K are set to a count of zero. (This comprised a very small percentage of the data, mostly

[4] One notable exception is desert regions, where extreme arid conditions and high evaporation can bring carbonates to the surface, forming a smooth, flat surface known as *caliche*.

[5] See Cavalieri et al. (1984) and Gloersen and Cavalieri (1986) for a complete description of this process.

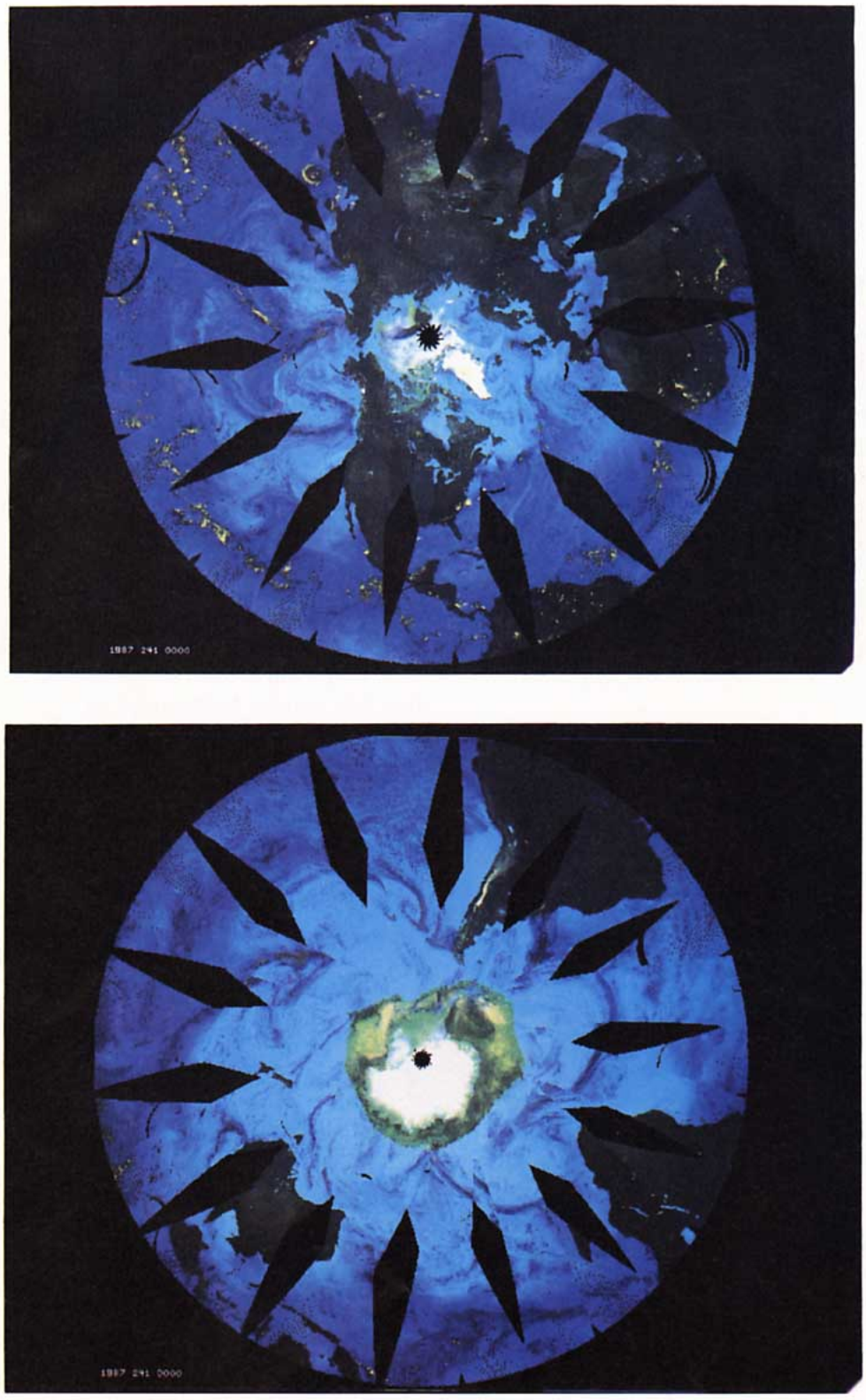

FIG. 1. Polar stereographic projections of brightness temperatures from the Special Sensor Microwave/Imager (SSM/I). Data from the 85.5 GHz vertically and horizontally polarized channels, and the 37.0 GHz vertically polarized channel are, respectively, displayed through the red, green and blue guns of a color monitor. Shown are both the ascending and descending orbits on 29 August 1987. Top figure is for the Northern Hemisphere, bottom figure for the Southern Hemisphere. Note Typhoon Dinah in the top figure, off the east coast of China.

TABLE 2. Description of features in the false-color SSM/I imagery. Temperature ranges observed during Northern Hemisphere summer conditions.

Feature*	Color	Brightness Temperature (K) 85.5 GHz (V) (red gun)	85.5 GHz (H) (green gun)	37.0 GHz (V) (blue gun)
Water surfaces				
Dry atmosphere	light blue	234–270	171–246	196–240
Moist atmosphere	dark blue	271–283	247–265	196–240
Land surfaces				
Snow cover	white/grey	174–270	182–225	221–260
Land (non-desert)	grey/brown	271–279	256–271	261–284
Deserts	light green	279–300	272–292	285–300
Other surfaces				
Polar snow/ice	white/yellow	157–247	152–221	170–239
Sea ice	green/brown	248–263	222–265	240–259
Clouds/precipitation				
Scattering (by cloud ice)	yellow	91–237	89–227	197–272
Emission (over water)	black	263–283	260–278	220–267

* Determined subjectively.

in summer hemisphere interior continental areas). In the false-color technique used to produce the cover figure and figure 1, the intensity of the red gun is "inversely" related (through C) to the 85.5 GHz vertically polarized T_B. Similarly, the intensity of the green and blue guns are, respectively, "inversely" related to the 85.5 GHz horizontally polarized channel and the 37.0 GHz vertically polarized channel. Thus, at each frequency, cold features appear bright and warm features appear dark. The scattering signature typified by low temperatures at 85.5 GHz results in high counts displayed through the red and green guns, a combination that produces the color yellow. Table 2 contains a summary of the important features, their associated colors, and their (frequency-dependent) temperature ranges. This temperature information is also diagrammed graphically in figure 2. The determination of "features" in table 2 is subjective, but is based on the fundamentals presented in section 2 and on geographical considerations.

The images on the cover are generated pixel for pixel from the 85.5 GHz data (12.5 km) full resolution, while the 37.0 GHz data (25 km full resolution) have each line and sample replicated. The data are unmapped; the conical scans of the SSM/I (see Hollinger et al. 1987, figure 2.8) are represented as (straight) image scan lines. Thus, some distortion of shape and distance occurs. Several missing scan lines cause discontinuities over Korea (left image) and southern Canada and Mexico (center image).

The leftmost cover image shows Typhoon Thelma at 2130 UTC 11 July 1987, when its maximum surface winds were reported to be between 120 and 130 kts. Light blue represents low brightness temperature with large differences between the horizontal and vertical polarizations, typical of clear oceanic regions. The dry air off the east coast of China is depicted by these light hues of blue, with progressively

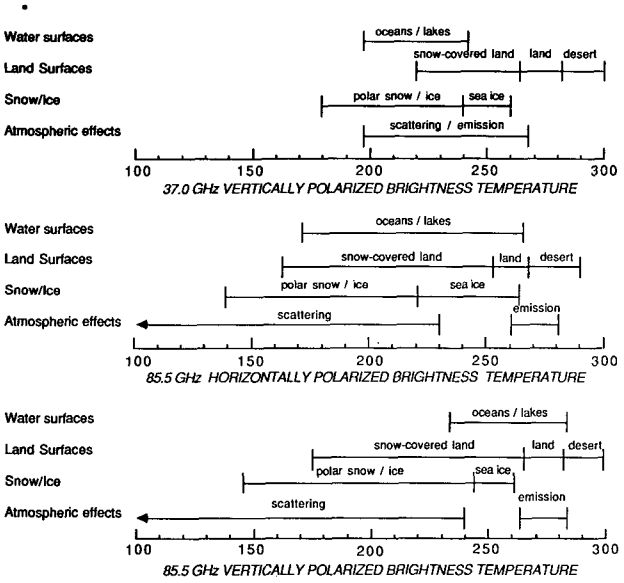

FIG. 2. Microwave brightness temperature ranges of various geophysical parameters observed during Northern Hemisphere summertime conditions. Arrows indicate that the temperature range extends beyond the indicated range.

more moist air or cloudy air shown by the darker blue hues. As the moisture and cloud water increase around the hurricane, the amount of thermal emission by the constituents increases, effectively both increasing the brightness temperature and reducing the polarization differences. This produces the darker shades of blue in the images. Light rain further increases the brightness temperature, and appears as the very dark blue to black regions. In the intense convective rainbands, the scattering of microwave radiation by ice particles dominates, causing low T_B (175 K) at 85.5 GHz. The low T_B results in high values being displayed through the red and green inputs, and thus the scattering process appears yellow. At 85.5 GHz, even moderate amounts of ice (300 gm · m^{-2} vertically integrated

ice content) completely mask any surface effects, hence convective features appear over the Asian continent as well.

An excellent example of the scattering process over land is to be seen in the center cover image—a squall line observed at 0100 UTC 17 August 1987. This line extends from Lake Michigan southward to central Texas and Mexico, and displays the cellular characteristics of a radar-observed squall line. At 85.5 GHz, where T_B as low as 94 K were observed in the cores of the storms, thin cirrus is very transparent. (Hakkarinen and Adler 1988, Spencer et al. 1988). The infrared-observed anvil would extend beyond the feature observed at 85.5 GHz (Adler et al. 1987).

The false-color display (cover, right) portrays an extratropical cyclone observed at 0940 UTC 17 January 1988. As mentioned previously, dry air overlying the ocean surface is seen as pale blue. Much of this air is found behind the cold front and wrapped into the center of the cyclone. The thermal emission by water vapor, cloud water, and rain water contribute to the darker blue shades. Embedded convective cores (yellow) characterize the scattering processes at 85.5 GHz, as clouds grow above the freezing level. The white dots north of the cyclone center are postulated as being due to scattering at 85.5 GHz, without apparent emission or scattering at 37 GHz; only cold, clear ocean is seen at 37 GHz.[6] North of Nova Scotia and the St. Lawrence Seaway one finds snow-covered land (white-yellow) and adjacent sea ice (green-brown) off the Labrador coast. Newfoundland stands out with complete snow-cover.

Figure 1 presents Hemispheric projections of SSM/I radiances observed on 29 August 1987, using the same false-color algorithm as used to produce the cover illustrations. The images are displayed at 25 km resolution in all channels, and the ascending (6 A.M.) and descending (6 P.M.) orbits have been combined. Note that global coverage is not quite complete in 24 hours. Note also that when two orbits view the same area, the later one (in time) is displayed. The small dot-like holes in the data near the equator are due to the remapping algorithm, but note that size of each "dot" represents the pixel area of 25 km. The Inter-Tropical Convergence Zone (ITCZ) is clearly apparent in the Northern Hemisphere image due to scattering (yellow), as is Typhoon Dinah off the east coast of China. At high latitudes, the atmospheric dryness is evident as the pale blue shades (dry air overlying the low T_B of the ocean surface). Over Greenland and the polar regions, snow cover and first-year and multi-year ice are apparent, as are the Himalayas (whitish-gray area). The desert regions of Africa and Saudi Arabia stand out as lighter shades of green. This phenomenon is due to the polarization of 86 GHz radiation by the smooth desert surface and is known as *caliche*. Observations of the Saudi Arabian desert from the SSM/I at 85.5 GHz show polarization differences of 15 K, compared to small polarization differences in central Europe.

In the Southern Hemisphere, Antarctica (white) and the surrounding sea ice (greenish yellow) are readily discernible, as is the overall atmospheric dryness (light blue) of the winter hemisphere. Fronts and cyclones in the westerlies are seen as the darker shades of blue due to the warming by emission over the cold ocean surface. Very little scattering by precipitation ice (i.e., convective processes) is apparent in this Hemisphere. The snow cover in the Andes might be interpreted as convection without prior knowledge of the geography and physics. Lake Titicaca and other high-altitude lakes in the Andes are visible as pale blue areas along the South American coast.

In summary, a rudimentary knowledge of microwave emission and scattering effects, combined with a knowledge of geography, lead to rapid identification of features in the SSM/I imagery. The false-color technique facilitates this assimilation by assigning a color or color-shade to various geophysical phenomena.

4. Summary

Microwave brightness temperatures at 85.5 GHz (vertical and horizontal polarizations) and at 37 GHz (vertical polarization) were displayed through the red, green, and blue guns of a color monitor. The resultant images highlighted qualitatively geophysical parameters important to a wide range of disciplines. Land-ocean differences, precipitation processes, and structure over land and water, surface characteristics, snow ice and sea ice were all discernible. Images such as those shown here are being used by the authors and others to select cases for more intensive study. For example, quantitative simulations and geophysical parameter retrieval schemes for parameters such as rainfall and hydrometeor distributions will be tested for identification of satellite-observed rain systems that near coastal radars such as those at Wallops Island, Virginia, Cape Canaveral, Florida, and Darwin, Australia. Another application of the SSM/I data will be to differentiate convective and stratiform rainfall, a step important to the estimation of the vertical profile of latent heating. Analysis of data from the SSM/I will also play a role in the design and testing of algorithms

[6] This difference may be due to the larger field of view at 37 GHz, which fails to detect small convective features; however further investigation is warranted.

for use in NASA's Tropical Rainfall Measuring Mission (Simpson et al. 1988) and in the Earth Observing System (NASA Advisory Council 1988).

Acknowledgments. The research in this article is supported through NASA's Mesoscale Atmospheric Research Program. The authors appreciate the support of the program's head, Dr. James Dodge, who has proposed real-time use of the SSM/I data through a NASA-sponsored network called WETNET. Informative discussions with Dr. Thomas Wilheit are also recognized.

References

Adler, R. F., N. Prasad, W. K. Tao, H. Y. Yeh, R. A. Mack, and J. Simpson. 1987. Microwave observations and modeling of deep convection. *Proceedings, International Symposium on Tropical Precipitation Measurements.* Tokyo, Japan.

Adler, R. F., W. K. Tao, N. Prasad, J. Simpson, and H. Y. Yeh. 1988. Satellite microwave rainfall simulations with a three-dimensional dynamical cloud model. AMS Preprint, Third Conference on Satellite Meteorology and Oceanography. Boston: American Meteorological Society, 290–295.

Cavalieri, D. J., P. Gloersen, and W. J. Campbell. 1984. Determination of sea ice parameters with the NIMBUS-7 SMMR. *J. Geophys. Res.* **89:** 5355–5369.

Colwell, R. N. 1983. *Manual of Remote Sensing, Volumes 1 and 2.* Falls Church (Virginia): American Society of Photogrammetry.

d'Entremont, R. P., and L. W. Thomason. 1987. Interpreting meteorological satellite images using a color-composite technique. *Bull. Amer. Meteor. Soc.* **68:** 762–768.

Gloersen, P., and D. J. Cavalieri. 1986. Reduction of weather effects in the calculation of sea ice concentration from microwave radiances. *J. Geophys. Res.* **91:** 3913–3919.

Hakkarinen, I. M., and R. F. Adler. 1988. Observations of precipitation convective systems at 92 and 182 GHz. *Meteor. Atmos. Phys.* **38:** 164–182.

Heymsfield, G. M., and R. Fulton. 1988. Comparison of high-altitude remote aircraft measurements with the radar structure of an Oklahoma thunderstorm: Implications for precipitation estimation from space. *Mon. Wea. Rev.* **116:** 1157–1174.

Hollinger, J., R. Lo, G. Poe, R. Savage, and J. Peirce. 1987. *Special Sensor Microwave/Imager User's Guide.* Washington, DC. Naval Research Laboratory.

Petersen, R. A., L. W. Uccellini, A. Mostek, and D. A. Keyser. 1984. Delineating mid- and low-level water vapor patterns in pre-convective environments. *Mon. Wea. Rev.* **112:** 2178–2198.

Prabhakara, C., D. A. Short, W. Wiscombe, R. S. Fraser, and B. E. Vollmer. 1986. Rainfall over oceans inferred from NIMBUS-7 SMMR: Application to the 1982–1983 El Niño. *J. Climate Appl. Meteor.* **25:** 1464–1474.

Short, N. M., P. D. Lowman, Jr., S. C. Freden, and W. A. Finch. 1976. *Mission to Earth: Landsat Views the World.* NASA Technical Report SP-360, National Aeronautics and Space Administration, Washington, DC.

Simpson, J., R. A. Adler, and G. R. North. 1988. A proposed tropical rainfall measuring mission (TRMM) satellite. *Bull. Amer. Meteor. Soc.* **69:** 278–295.

Spencer, R. W., H. M. Goodman, and R. E. Hood. 1988. Precipitation retrieval over land, and ocean with the SSM/I, Part 1: Identification and characteristics of the scattering signal. (Submitted to *J. Atmos. Ocean. Tech.*)

Spencer, R. W., W. S. Olsen, W. Rongzhang, D. W. Martin, J. A. Weinman, and D. A. Santek. 1983. Heavy thunderstorms observed over land by the NIMBUS-7 Scanning Multichannel Microwave Radiometer. *J. Climate Appl. Meteor.* **22:** 1041–1046.

Wilheit, T. T., J. L. King, E. B. Rodgers, R. A. Nieman, B. M. Krupp, A. S. Milman, J. S. Stratigos, and H. Siddalingaiah. 1982. Microwave radiometric observations near 19.35, 35, 92 and 183 GHz of precipitation in tropical storm Cora. *J. Appl. Meteor.* **21:** 1137–1145.

Wu, R. and J. A. Weinman. 1984. Microwave radiances from precipitating clouds containing aspherical ice, combined phase, and liquid hydrometeors. *J. Geophys. Res.* **89:** 7170–7178. ●